



Complementary study of heat capacity and magnetization for intermetallic $\text{YNi}_2\text{B}_2\text{C}$ single crystal

K.J. Song^{a,*}, C. Park^a, S.S. Oh^a, Y.K. Kwon^a, J.R. Thompson^{b,c},
D.G. Mandrus^{b,c}, D. McK. Paul^d, C.V. Tomy^e

^a Korea Electrotechnology Research Institute, Changwon, Kyungnam 641-120, South Korea

^b Department of Physics, University of Tennessee, Knoxville, TN 37919, USA

^c Solid State Division, Oak Ridge National Laboratory, Oak Ridge, TN 37919, USA

^d Department of Physics, University of Warwick, Coventry CV47AL, UK

^e Department of Physics, I.I.T. Powai, Mumbai 40076, India

Received 9 April 2003; accepted 23 May 2003

Abstract

The superconducting and magnetic properties of $\text{YNi}_2\text{B}_2\text{C}$ single crystal have been investigated by heat capacity and dc-magnetic methods, with magnetic field applied parallel to the c -axis, i.e., $H\parallel(001)$ -direction. In the framework of heat capacity and magnetization analyses, we obtain the thermodynamic critical field H_c from both heat capacity and magnetization data. The heat capacity data deviate from predictions for both weak- and strong-coupling superconductivity, but are described relatively well in a medium-coupling analysis. The precise t^3 -dependence of the electronic heat capacity C_{es} indicates the gap anisotropy with the presence of point nodes for $\text{YNi}_2\text{B}_2\text{C}$ single crystal.

© 2003 Elsevier B.V. All rights reserved.

PACS: 74.70.Dd; 74.25.Bt; 74.25.Ha

1. Introduction

The layered intermetallic compounds [1] $\text{RNi}_2\text{B}_2\text{C}$ (where R = lanthanide) have been studied with great attention by many research groups. The nickel borocarbide family exhibits a variety of interesting physical phenomena, including the co-existence of superconductivity and magnetism arising from magnetic moment of rare earth elements R; the transformation of the vortex (flux

line) lattice from the simple hexagonal to square symmetry; a fairly high superconducting transition temperature T_c comparable with several A-15 compounds, and so on [2–8]. Early work reported single crystal $\text{YNi}_2\text{B}_2\text{C}$, one of the quaternary intermetallic compounds, to be a conventional and an isotropic superconductor [9]. The analysis yielded the value $\kappa = 13\text{--}15$ for the GL-parameter, indicating a type-II superconductor [10]. However, recent works [11–13] have showed a large anisotropic gap function with point nodes. In addition, the upper critical field H_{c2} of $\text{YNi}_2\text{B}_2\text{C}$ single crystal has an unconventional behavior. Several research groups have found an upward, positive

* Corresponding author.

E-mail address: kjsong@keri.re.kr (K.J. Song).

curvature of H_{c2} at low temperature regime [14–16]. In magnetization studies, it is sometimes difficult to determine H_{c2} precisely, due both to the presence of paramagnetic signals in the normal and superconductive states and to an apparent deviation from simple London theory in the low temperature regime. This latter effect arises from non-local electrodynamics in clean materials (with a long electron mean free path) and is well described by a non-local formulation of London theory [6]. The anisotropic paramagnetic signal in the crystal studied here apparently arises from rare earth impurities in the yttrium starting material at a level of $\sim 0.1\%$ [8]. In this present work, we report results on the thermodynamic critical field H_c obtained by applying thermodynamics to both magnetization and heat capacity measurements. In addition, we discuss the results of heat capacity and the values of the coefficient of electronic heat capacity γ obtained by various ways. Furthermore, we validate $\text{YNi}_2\text{B}_2\text{C}$ single crystal has showed the presence of point nodes based on the t^3 -dependence of the electronic heat capacity C_{es} and has arranged relatively well to a medium-coupling analysis based on the coefficient of electronic heat capacity γ .

2. Experimental

Details of the experimental aspects have been presented elsewhere [6,8]. Here we report the results of complementary investigations of both the magnetization and the heat capacity in the normal and superconducting state, obtained in a commercial Quantum Design both 7-T SQUID magnetometer and 9-T PPMS instrument. Several features have been studied. The normal state magnetic properties with the field parallel to (001)-direction are investigated. The heat capacity in the normal state by applying a high magnetic field, in the superconducting state with a zero magnetic field, and in the intermediated state by applying a magnetic field are observed at low temperatures. From the framework of heat capacity and magnetization analyses, the coefficient of electronic heat capacity γ is estimated, and the thermodynamic critical field H_c is deduced as well.

3. Results and discussion

3.1. The magnetic susceptibility in normal state

The normal state magnetic susceptibility was measured between 16 and 295 K in a magnetic field of 10 kG parallel to the (001)-direction. Fig. 1 shows the magnetic susceptibility χ vs. $1/T$, while the inset shows the $1/\chi$ vs. T relationship for the (001)-direction of applied field. The total magnetic susceptibility χ is attributed both to localized and to delocalized conduction electrons. As shown in the inset of Fig. 1, the data for $T > 100$ K formally can be described by a Curie–Weiss expression,

$$\begin{aligned}\chi^{\text{molar}} &= N_A p^2 \mu_B^2 / 3k_B (T + \theta) = N_A \mu_{\text{eff}}^2 / 3k_B (T + \theta) \\ &= C / (T + \theta),\end{aligned}$$

where C is Curie constant, θ is Weiss temperature, N_A is Avogadro's number, k_B is Boltzmann constant, μ_B is Bohr magneton, and μ_{eff} is the effective magnetic moment per formula unit. The high temperature slope ($100 \text{ K} < T < 295 \text{ K}$) corresponds to a value of $1.83\mu_B$ for the effective magnetic moment in an applied field parallel to (001)-

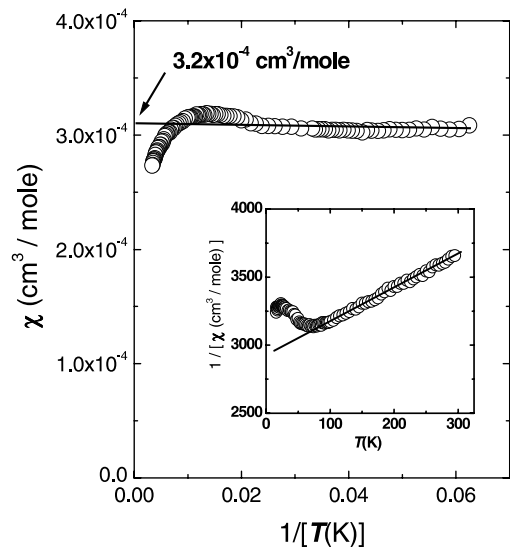


Fig. 1. The temperature dependence of magnetic susceptibility χ for the applied field parallel to (001)-direction. The inset shows $1/\chi$ vs. temperature T .

direction. This value is smaller than the theoretical value of $2.83\mu_B$ for the Hund's rule ground state of Ni^{2+} when the orbital moments are quenched due to crystalline electric field (CEF) effects. The Weiss temperature, θ , is found to be about 1235 K. Alternatively, in the main frame of Fig. 1, χ is nearly constant ($3.2 \times 10^{-4} \text{ cm}^3/\text{mol}$) and seems to be attributed in full to Pauli spin paramagnetism. The Pauli paramagnetism, however, varies somewhat with T , due to the presence of a DOS (density of state) peak near the Fermi level as shown by Lee et al. [17]. Therefore, the discrepancy of the effective magnetic moment may be explained by the variation of the Pauli paramagnetism and the Curie–Weiss impurity contribution.

The normal state paramagnetic signal from paramagnetic Ni^{2+} ions is very weak, compared with that arising from rare earth ions in $\text{RNi}_2\text{B}_2\text{C}$ compounds. In the $\text{YNi}_2\text{B}_2\text{C}$ compound, however, the paramagnetic signal due to Ni^{2+} ions could be a significant factor, because the Y as well as B and C are non-magnetic elements. In addition, the deviations from Curie–Weiss behavior and the large Weiss temperature may indicate that the Ni 3d bands are delocalized and contribute to the conduction electron states. Electron band structure calculations for $\text{RNi}_2\text{B}_2\text{C}$ materials [18–20] show that the bands near the Fermi level display predominant Ni 3d bands, with a relatively high density of states at E_F , and that the superconductivity may come from a conventional mechanism with strong electron–phonon coupling, in contrast to implications of the analysis of Lee et al. [17] who obtained convincingly a medium-coupling superconductivity based on the coefficient of electronic heat capacity γ over the calculated DOS for $\text{YNi}_2\text{B}_2\text{C}$. However, recent work has shown the superconducting energy gap to be strongly anisotropic, but always gapped [11–13], as indicated to unconventional superconductivity.

3.2. Heat capacity in normal and superconducting state

Now we consider the heat capacity of the compound and compare the results with several models. Fig. 2 plots the heat capacity C_p/T as a function of T^2 for the single crystal $\text{YNi}_2\text{B}_2\text{C}$. All

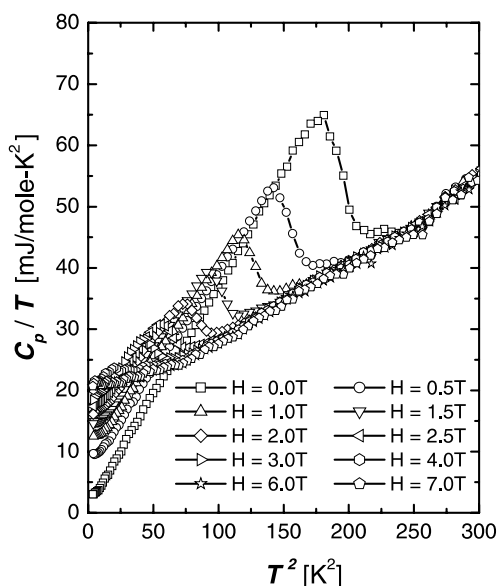


Fig. 2. C_p/T vs. T^2 for the single crystal $\text{YNi}_2\text{B}_2\text{C}$.

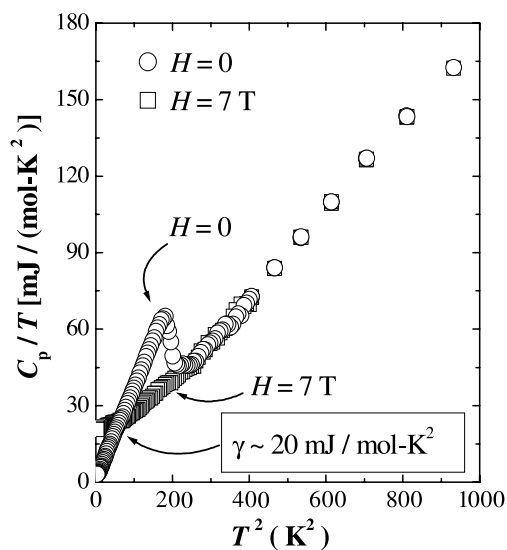


Fig. 3. C_p/T vs. T^2 in the temperature regime 20–30 K for normal state under applying $H = 70 \text{ kG}$ and superconducting state with zero magnetic field.

measurements have been done in the field cooling conditions. Specially, Fig. 3 shows the heat capacity C_p/T as function of T^2 in the temperature regime from 2 to 30 K for the normal state ($H = 70 \text{ kG}$) and superconducting states ($H = 0 \text{ G}$). In

zero fields, there is a jump of heat capacity at $T_c \approx 14.5$ K. The jump disappears in high field $H = 70$ kG, which exceeds H_{c2} . In the normal state ($H = 70$ kG), the heat capacity C_p (in the temperature range $2 \text{ K} < T < 14 \text{ K}$) can be fit to the relation of $C_p/T = \gamma + \beta T^2$ (or $\gamma + \beta T^2 + \delta T^4$), where γ is the coefficient of the electronic heat capacity (Sommerfeld parameter) and β the lattice heat capacity. The deviations (δ) from the T^3 asymptotic behavior come from the fact that the phonon DOS for crystalline solids shows deviations with respect to the Debye DOS, which is derived for an elastic continuum. Without the deviations term (δT^4), we obtain $\gamma \approx 19.1 \text{ mJ}/(\text{mol K}^2)$ and $\beta \approx 0.097 \text{ mJ}/(\text{mol K}^4)$; with the deviations term, we have $\gamma \approx 20.6 \text{ mJ}/(\text{mol K}^2)$, $\beta \approx 0.037 \text{ mJ}/(\text{mol K}^4)$, and $\delta \approx 0.00033 \text{ mJ}/(\text{mol K}^6)$. The result for the electronic term γ is similar to the values found by other groups [21,22]. We can obtain the value of the Debye temperature by $\beta = 1944Z/\Theta_D^3$ (where Z is the number of atoms per formula unit); $\Theta_D \approx 495$ K without and $\Theta_D \approx 680$ K with the deviations term. The flattening of the curve of C/T vs. T^2 in Fig. 3 and the apparent deviations have been attributed to the presence of low-lying phonon modes [23].

We use the γ values to check for consistency in various analyses. There are number of BCS and GLAG relationships between the normal and superconductive state properties [24]:

$$-(dH_{c2}/dT)_{T_c} = 9.55 \times 10^{24} \gamma^2 T_c (n^{2/3} S/S_F)^2 [\text{G/K}]$$

(in the clean limit),

$$\lambda_{L0} = 1.33 \times 10^8 \gamma^{1/2} (n^{2/3} S/S_F)^{-1} [\text{cm}]$$

(at $T = 0$ K),

where γ is the coefficient of the normal-state electronic heat capacity, n is the conduction-electron density, S is Fermi surface, S_F is the Fermi surface of an electron gas of density n , and λ_{L0} is London penetration depth at 0 K. In the collection of relations, there are only four independent quantities [24]. Experimentally, however, we have in effect “over-determined” the system by measuring more quantities than this. From our magnetization results $-(dH_{c2}/dT)_{T_c} \approx 3400 \text{ G/K}$, $\lambda_{L0} \approx 89.5 \times 10^{-7} \text{ cm}$, and $T_c = 14.5$ K, we obtain $\gamma \approx 5420 \text{ erg/}$

$(\text{cm}^3 \text{K}^2) \approx 21.5 \text{ mJ}/(\text{mol K}^2)$, which compares very well with our direct evaluation. These results fairly agree well to the fitting value of normal-state heat capacity. From γ and the jump of the zero field heat capacity data, we get $\Delta C_p/(\gamma T_c) \approx 1.81$, which significantly exceeds the BCS weak-coupling ratio, 1.43.

To compare further the predictions of the BCS theory with heat capacity measurement, we focus on the electronic heat capacity C_{es} in the superconducting state. Assuming that the lattice heat capacity in the normal C_{ln} and superconducting state C_{ls} are the same, $C_{ln} = C_{ls} = \beta T^3$ (which was obtained from measurements above and below T_c), we obtain C_{es} by subtracting the lattice heat capacity in normal state (C_{ln} ; $H = 70$ kG) from the total heat capacity in the superconducting state (C_p ; $H = 0$ G) below T_c ; so $C_{es} = C_p - C_{ln}$. A plot of C_{es} vs. T is shown at Fig. 4. These data for C_{es} vs. T follow a t^3 dependence to surprising accuracy, where $t = T/T_c$ is the reduced temperature; this is shown in the inset of Fig. 4, a plot of C_{es} vs. t^3 . The precise t^3 -dependence of the electronic heat capacity C_{es} indicates the gap anisotropy with the presence of point nodes as shown in recent works [11–13]. A similar t^3 -dependence has been reported

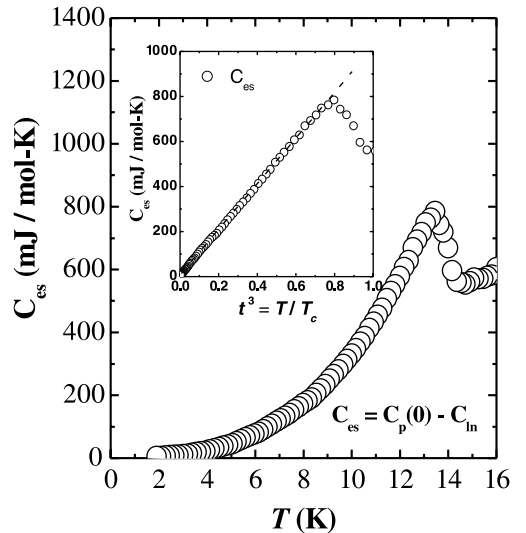


Fig. 4. The electronic heat capacity C_{es} vs. temperature T in superconducting state. The inset shows the t^3 -dependence of C_{es} .

by Hong, et al. for their compounds [25]. In fact, this t^3 temperature dependence arises in the two fluid model, which contains a parabolic variation of the thermodynamic critical field H_c with temperature; the model relates H_c to the coefficient of electronic heat capacity via $\gamma = H_0^2/(2\pi T_c^2)$ where $H_0 = H_c(0)$. The two-fluid model gives the following simple relations appropriate to medium-coupling superconductors, with electron–phonon coupling constant $\lambda \approx 1$ [26]:

$$C_{es} = 3\gamma T_c t^3, \quad \text{where } t = T/T_c,$$

$$\Delta C/\gamma T_c = 2,$$

$$d(C_{es}/T)/dT = 6\gamma/T_c \quad (\text{at } T = T_c).$$

From the C_{es} data, we can again deduce values for γ and obtain $\gamma \approx 23.1$ [mJ/mol K²] from the first relation using $d(C_{es})/d(t^3) \approx 1010$ [mJ/mol K]; also we get $\gamma \approx 18.6$ [mJ/mol K²] from $\Delta C \approx 540$ [mJ/mol K]; and finally $\gamma \approx 19.0$ [mJ/mol K²] from $d(C_{es}/T)/dT \approx 7.85$ [mJ/mol K³]. These values for γ are relatively consistent ($\pm \sim 10\%$) with the direct fit to the normal-state heat capacity and the value calculated from magnetization data. The above results seem to be consistent with the medium-coupling analysis.

3.3. Thermodynamic critical field

For both type-I and -II superconductors, the thermodynamic critical field H_c is defined by the relation,

$$H_c^2(T)/8\pi = [F_n(T) - F_s(T)]/V_{\text{molar}},$$

where $F_n(T)$ (or $F_s(T)$) is molar free energy of the normal state (or superconducting state), V_{molar} is molecular volume. In addition, the molar specific heat is defined by $C_p = T[dS/dT]$. Finally, one obtains for superconductors,

$$\begin{aligned} C_n - C_s &= T(\partial/\partial T)[S_n(T) - S_s(T)] \\ &= -(TV_{\text{molar}}/8\pi)(\partial^2/\partial T^2)[H_c(T)]^2, \end{aligned}$$

where C_n , S_n , and F_n are the specific heat, entropy, and free energy of the normal state, and C_s , S_s , and F_s refer to the superconducting state. Using thermodynamics, we can derive H_c from the specific heat experiment with the following:

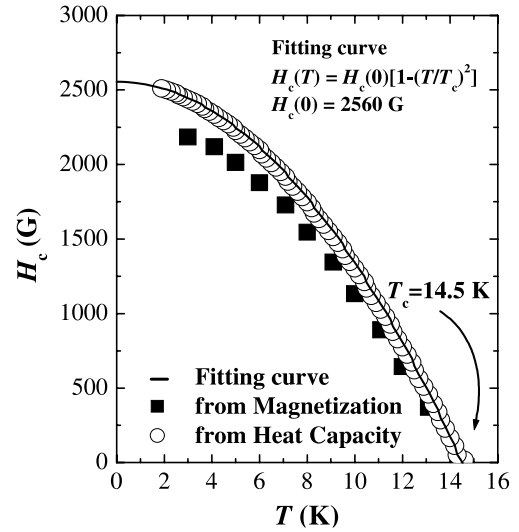


Fig. 5. The temperature dependence of critical field H_c . The fitting curve is given by $H_c(T) = H_c(0)[1 - (T/T_c)^2]$, according to heat capacity results, where $H_c(0)$ is about 2556 G, T_c is 14.5 K. Open squares result from heat capacity, and close squares come from magnetization analysis.

$$\begin{aligned} H_c^2(T) &= (8\pi/V_{\text{molar}}) \\ &\times \int_T^{T_c} dT' \int_{T'}^{T_c} dT'' \{ [C_s(T'') - C_n(T'')]/T'' \}. \end{aligned}$$

The resulting temperature dependence of H_c is shown in Fig. 5. The solid line shows that a parabolic dependence $H_c(T) = H_c(0)[1 - (T/T_c)^2]$ describes the data well, yielding $H_c(T=0) \approx 2556$ G. Near T_c , the slope of H_c is $-(dH_c/dT)_{T_c} \approx 320$ G/K. From an empirical relation for the superconducting energy gap $\Delta(0)$ [27],

$$-[(T/H_c(0))(dH_c(T)/dT)]_{T=T_c} = \Delta(0)/k_B T_c,$$

we estimate $\Delta(0)/k_B T_c \approx 1.82$, giving an energy gap $\Delta(0) \approx 2.26$ meV. Thus the data are described reasonably well, with $\Delta(0)/k_B T_c$ exceeds somewhat the BCS value, 1.77. The t^3 -dependence of C_{es} implies a parabolic variation of thermodynamic critical field H_c with temperature, as we have shown in Fig. 5. So good as the t^3 -dependence of C_{es} , the coefficient of electronic heat capacity $\gamma = (1/2\pi)(H_0^2/T_c^2)$ is reasonable approximation (≈ 19.6 [mJ/mol K²], where $H_0/H_c(0) \approx 2556$ G).

This fairly agrees well to previous results. On the other hand, strong-coupling theory predicts that $\Delta(0)/(k_B T_c) = 1.76[(\Delta C_p/\gamma T_c)/1.43]^{1/2}$ as shown by Leggett [28]. Taking the measured $\Delta C_p/(\gamma T_c) \approx 1.81$ with $\gamma \approx 20$ [mJ/mol K²] for our crystal, the term $1.76 [(\Delta C_p/\gamma T_c)/1.43]^{1/2} \approx 1.98$, which significantly exceeds the value $\Delta(0)/k_B T_c \approx 1.82$. Therefore, strong-coupling theory does not appear appropriate to the heat capacity results on this YNi₂B₂C single crystal.

Let us consider now the magnetization in the superconducting state, with is remarkably reversible overall [6,8]. At relatively low temperatures ($\approx T_c/3$), there are still wide reversible regions, which allows one to apply thermodynamics with some accuracy. Whatever is the shape of the equilibrium magnetization curve, the area under the curve gives the condensation energy, $H_c^2/8\pi$. Thus one has

$$-\int M dH = F_n(0) - F_s(0) = H_c^2/8\pi.$$

Experimentally, the magnetization of the crystal is not completely reversible at low fields, so we need to approximate M_{eq} in this region. Previously we showed that the magnetization curves $M(H)$ at low temperature region deviate markedly from the simple $\ln(H)$ dependence of local London theory, but are well-described by its extension to incorporate effects on non-local electrodynamics. Thus, we have taken the magnetization $M(H)$ from a non-local London analysis as described previously [6]. Specially, the contribution at low fields is estimated by extrapolating an $M(H)$ curve to lower fields until it intersects the Meissner-slope curve. The areas under the Meissner line and under the extrapolated curve are added to a direct numerical integration of the experimental M_{eq} at higher fields, to obtain the total area under the magnetization curve. The resulting values of $H_c(T)$ are shown in Fig. 5. The overall shape and temperature dependence are very similar for the $H_c(T)$ from heat capacity and from magnetization. However, the latter curve lies $\sim 8\%$ lower at all temperatures. This may be due to the approximations cited or to some other experimental artifact.

4. Summary

In the framework of heat capacity and magnetization analyses, the thermodynamic critical field, H_c , of our single crystal of YNi₂B₂C is described well, with deduced value $\Delta(0)/k_B T_c \approx 1.82$. The $H_c(T)$ accurately follows a parabolic dependence $H_c(T) = H_c(0)[1 - (T/T_c)^2]$, with $H_c(0) \approx 2556$ G. We validate qualitatively the gap anisotropy with the presence of point nodes based on the t^3 -dependence of the electronic heat capacity C_{es} for our single crystal of YNi₂B₂C. From another aspect, we confirm the heat capacity data, based on the coefficient of electronic heat capacity γ estimated by various ways, deviate from predictions of both the weak- and strong-coupling theory, but are fairly well described by medium-coupling relationships, as shown from band calculation by Lee et al. [17]. The present study does not, of course, have microscopic evidence for a medium-coupling mechanism. We have a reasonably self-consistent analysis of heat capacity, magnetic susceptibility, and magnetization experimental investigations, obtaining values for the coefficient of electronic heat capacity $\gamma \approx 20$ [mJ/mol K²], with medium-coupling theory being most appropriate. Overall, the non-magnetic borocarbide superconductors have revealed much surprising physical behavior and may yet contain future surprises.

Acknowledgements

The author (K.J. Song) wishes to acknowledge supporting by the Korea Electrotechnology Research Institute and thanks to a reviewer for valuable comments. The Oak Ridge National Laboratory is managed by UT-Battelle, LLC for the US DOE under contract DE-AC-00OR22725.

References

- [1] R.J. Cava, H. Takagi, H.W. Zandbergen, J.J. Krajewski, W.F. Peck, T. Siegrist, B. Batlogg, R.B. Van Dover, R.J. Felder, K. Mizuhashi, J.O. Lee, H. Eisaki, S. Uchida, Nature (London) 367 (1994) 252.
- [2] U. Yaron, P.L. Gammel, A.P. Ramirez, D.A. Huse, D.J. Bishop, A.I. Goldman, C. Stassis, P.C. Canfield, K.

- Mortensen, M.R. Eskildsen, *Nature (London)* 382 (1996) 236.
- [3] P.C. Canfield, B.K. Cho, D.C. Johnston, D.K. Finnemore, M.F. Hundley, *Physica C* 230 (1994) 397.
- [4] M.R. Eskildsen, P.L. Gammel, B.P. Barber, U. Yaron, A.R. Ramirez, D.A. Huse, D.J. Bishop, C.A. Bolle, C.M. Lieber, S. Oxx, S. Sridhar, N.H. Anderson, K. Mortensen, P.C. Canfield, *Phys. Rev. Lett.* 78 (1997) 1968.
- [5] D. McK. Paul, C.V. Tomy, C.M. Aegerter, R. Cubitt, S.H. Lloyd, E.M. Forgan, S.L. Lee, M. Yethiraj, *Phys. Rev. Lett.* 80 (1998) 1517.
- [6] K.J. Song, J.R. Thompson, M. Yethiraj, D.K. Christen, C.V. Tomy, D. McK. Paul, *Phys. Rev. B* 59 (1999) R6620.
- [7] L. Civale, A.V. Silhanek, J.R. Thompson, K.J. Song, C.V. Tomy, D. McK. Paul, *Phys. Rev. Lett.* 83 (1999) 3920.
- [8] J.R. Thompson, A.V. Silhanek, L. Civale, K.J. Song, C.V. Tomy, D. McK. Paul, *Phys. Rev. B* 64 (2001) 024510.
- [9] E. Johnston-Halperin, J. Fiedler, D.E. Farrell, M. Xu, B.K. Cho, P.C. Canfield, D.K. Finnemore, D.C. Johnston, *Phys. Rev. B* 51 (1995) 12852.
- [10] M. Xu, P.C. Canfield, J.E. Ostenson, D.K. Finnemore, B.K. Cho, Z.R. Wang, D.C. Johnston, *Physica C* 227 (1994) 321.
- [11] M. Nohara, H. Suzuki, N. Mangkorntong, H. Takagi, *Physica C* 341–348 (2000) 2177.
- [12] K. Izawa, A. Shibata, Y. Matsuda, Y. Kato, H. Takeya, K. Hirata, C.J. van der Beek, M. Konczykowski, *Phys. Rev. Lett.* 86 (2001) 1327.
- [13] K. Izawa, K. Kamata, Y. Nakajima, Y. Matsuda, T. Watanabe, M. Nohara, H. Takagi, P. Thalmeier, K. Maki, *Phys. Rev. Lett.* 89 (2002) 137006-1.
- [14] S.B. Roy, Z. Hossain, A.K. Pradhan, P. Chaddah, R. Nagarajan, L.C. Gupta, *Physica C* 256 (1996) 90.
- [15] S.V. Shulga, S.L. Drechsler, G. Fuchs, K.H. Muller, K. Winzer, M. Heinecke, K. Krug, *Phys. Rev. Lett.* 80 (1998) 1730.
- [16] M.-O. Mun, M.-S. Kim, S.-I. Lee, B.K. Cho, I.-S. Yang, W.C. Lee, P.C. Canfield, *Physica C* 303 (1998) 57.
- [17] J.I. Lee, T.S. Zhao, I.G. Kim, B.I. Min, S.J. Youn, *Phys. Rev. B* 50 (II) (1994) 4030.
- [18] W.E. Pickett, D.J. Singh, *Phys. Rev. Lett.* 72 (1994) 3702.
- [19] D.J. Singh, W.E. Pickett, *Phys. Rev. B* 51 (1995) 8668.
- [20] L.F. Mattheiss, *Phys. Rev. B* 49 (1994) 13279.
- [21] H. Michor, T. Holubar, C. Dusek, G. Hilscher, *Phys. Rev. B* 52 (1995) 16165.
- [22] R. Movshovich, M.F. Hundley, J.D. Thomson, P.C. Canfield, B.K. Cho, A.V. Chubukov, *Physica C* 227 (1994) 381.
- [23] G. Hilscher, H. Michor, in: A.V. Narlikar (Ed.), *Superconductivity and Magnetism in Quaternary Borocarbides and Boronitrides, Studies of High Temperature Superconductors*, vol. 28, Nova Science Publishers, New York, 1999, p. 1.
- [24] T.P. Orlando, E.J. McNiff Jr., S. Foner, M.R. Beasley, *Phys. Rev. B* 19 (1979) 4545.
- [25] N.M. Hong, H. Michor, M. Vybornov, T. Holubar, P. Hundegger, W. Perthold, G. Hilscher, P. Rogl, *Physica C* 227 (1994) 85.
- [26] D.M. Ginsberg, *Physical Properties of High Temperature Superconductors II*, World Scientific Publishing Company, 1990, p. 13.
- [27] A.M. Toxen, *Phys. Rev. Lett.* 15 (1965) 462.
- [28] A.J. Leggett, *Rev. Mod. Phys.* 47 (1975) 331.